Development of a Vertically Configured MEMS Heat Flux Sensor

Antti Immonen, *Member, IEEE*, Saku Levikari, *Member, IEEE*, Feng Gao, Pertti Silventoinen, *Member, IEEE*, and Mikko Kuisma, *Member, IEEE*

***Abstract*— Heat flux sensors (HFSs) have potential in enabling applications that require direct and instantaneous tracking of thermal energy transfer. To facilitate the widespread use of the sensors, the sensors have to be robust and feasible to implement, while maintaining high sensitivity, fast response time, and low thermal obtrusiveness. However, most of the currently available HFSs are either challenging to manufacture or ill-suited for surface heat flux measurement because of their mechanical or thermal characteristics. In this article, the design of a novel microelectromechanical systems (MEMS) HFS structure intended for surface heat flux measurements is presented. A prototype batch is manufactured and the electrical performance of the prototype sensors is compared with commercially available HFSs. Results show that sensors with similar sensitivity as commercial sensors can be made by using MEMS methods.**

***Index Terms*— 3-D, heat flux, microelectromechanical systems (MEMS), sensor, thermopile.**

I. Introduction

DIRECT measurement of heat transfer is being utilized in a growing number of applications over various fields of industry and science. Although traditional temperature measurements can be used to infer the magnitude of heat transfer under certain conditions, they are often insufficient in terms of accuracy or impractical to execute. In such situations, the use of a heat flux sensor (HFS) is often preferred [1], [2].

An HFS is a device that enables direct measurement of the flow of heat, even in the presence of multiple heat coupling mechanisms [3], including conduction, radiation and convection [4]. HFSs are often based on differential temperature measurement across the sensor itself, resolving temperature differences on the order of microkelvins [1]. This, in combination with a small physical size and a low thermal mass, facilitates the HFSs to track heat transients even on the submicrosecond scale [2]. The most common type of discrete HFS is a thermoelectric transducer, which converts a temperature difference directly into a voltage by the Seebeck effect [4].

Manuscript received July 30, 2020; revised September 30, 2020; accepted October 9, 2020. Date of publication October 30, 2020; date of current version January 7, 2021. This work was supported in part by Business Finland under Project Q-Health and in part by the Academy of Finland under Project THERAD. The Associate Editor coordinating the review process was Tarikul Islam. *(Corresponding author: Antti Immonen.)*

Antti Immonen, Saku Levikari, Pertti Silventoinen, and Mikko Kuisma are with the LUT School of Energy Systems, Lappeenranta University of Technology, 53850 Lappeenranta, Finland (e-mail: antti.immonen@lut.fi).

Feng Gao is with the VTT Technical Research Centre of Finland Ltd., 02150 Espoo, Finland (e-mail: feng.gao@vtt.fi).

Digital Object Identifier 10.1109/TIM.2020.3034961

The ability to instantaneously track changes in heat transfer in a noninvasive way has resulted in a wide range of applications for HFSs. For example, HFSs have been used for direct vaporization enthalpy measurement [5], combustion measurements [3], thermal monitoring of power electronics [6], skin surface heat flux-based energy expenditure and core body temperature monitoring [7], [8], battery charging monitoring [9], and building energy performance assessment [10].

Despite the technical benefits of direct heat flux measurement in a wide range of applications, HFSs are employed relatively rarely in the industry and are currently largely limited to research applications [4]. Instead of using discrete HFS elements, the transfer rate of heat is typically calculated based on one or more temperature measurements [2], [11]. According to [4], the scarce popularity of discrete HFSs is most likely a result of the relatively high cost and challenging manufacturability, as well as the low awareness of the capabilities of the technology. To realize new or improved thermal measurement applications in a surface measurement setting, robust, cost-effective, and scalable sensor designs are needed.

In this article, a novel 3-D HFS structure for surface heat flux measurement is proposed. The designed structure is simulated by the finite element method and manufactured using a customized microelectromechanical systems (MEMS) fabrication process. Finally, the thermoelectric performance of the sensor prototype is evaluated experimentally, and prospective industrial uses for the sensors are discussed.

This article is extended from a conference publication presented at IEEE I^{2}MTC 2020 [12].

II. Thermopile Heat Flux Sensors

Heat flux $\bar{q}$ describes the transfer of thermal energy, that is, heat, by means of conduction, convection, or radiation. In the case of conduction through a medium with thermal conductivity k, the heat flux density can be expressed by the temperature gradient ∇T according to Fourier's law [1] as

$$\bar{q} = -k\nabla T. \tag{1}$$

Thus, the total heat flux through a surface can be expressed by multiplying the heat flux density in (1) by the surface area.

Heat flux is commonly measured indirectly by monitoring the effects of heat conduction in a medium with known characteristics of thermal conduction [13]. This can be done by applying a differential temperature measurement across a thermal resistance layer and calculating the heat transfer rate based

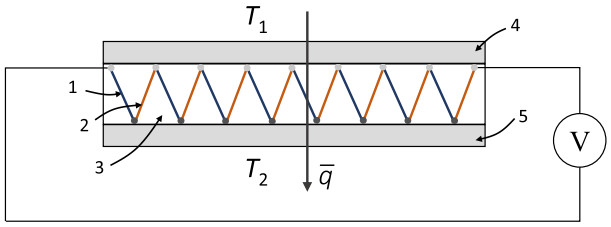

Fig. 1. Thermopile HFS, composed of multiple thermocouple legs (1 and 2) in series. The voltage output corresponds to the heat flux $\overline{q}$ conducted through the heat resistance of the sensor active layer 3. In practical constructions, the sensors often include heat spreader support plates 4 and 5.

on Fourier's law [11]. In practice, this can be accomplished with application-specific surface-mounted HFS plates, which incorporate a differential temperature measurement and a heat resistance layer in one calibrated package [11]. However, this approach requires knowing the thermal conductivity of the heat resistance layer very precisely [1]. Moreover, when the size and thickness of the sensor are scaled down, the decreasing temperature difference of the two temperature sensors becomes more difficult to measure accurately. Other HFS designs employ thermoelectric effects for generating voltage directly from the temperature difference by using structures known as thermopiles [2]. Although a number of widespread transducer technologies can be regarded as HFSs, this article focuses on contact-type thermopile sensors in the form factor of a plate.

A. Sensor Operation

Discrete HFSs are commonly implemented as passive elements employing the Seebeck effect for direct temperature difference measurement [4]. In short, the Seebeck effect refers to the generation of an electromotive force in a material, resulting from a temperature gradient across the material. In other words, when a conductor is heated from one end, a voltage is induced along the length of the conductor, either codirectionally or opposite to the flow of heat [1].

Thermopile HFSs utilize this property and are built by electrically series connecting alternating types of thermoelectric legs that are connected thermally in parallel to sum the generated voltages of individual legs into a useful amplitude [14], [15]. The operation and main component parts of a conventional thermopile HFS are illustrated in Fig. 1.

The operation of an HFS is mainly characterized based on its ability to convert the through-traversing heat flux to an electrical signal [3]. The sensitivity of the sensor S_0 is usually given as a ratio of the total thermoelectromotive force output $\mathcal{E}_{\text{emf}}$ to the heat flow per unit area q

$$S_0 = \frac{\mathcal{E}_{\text{emf}}}{q} = \frac{h\, n_{\text{j}}\, S}{k} \tag{2}$$

where h and k are the thickness in meters and thermal conductivity in W/(m · K) of the sensing layer, respectively, S is the average Seebeck coefficient of a single thermoelectric leg in the device, in V/K, and n_{j} is the number of the thermoelectric legs [13]. The voltage output signal of the sensor is thus directly dependent on how much the sensor thermally impedes the heat flow, and the number and unit thermopower of the thermoelectric legs situated inside the thermal resistance, that is, $U_{\text{out}} = q\, S_0$.

In addition to directly measuring steady-state heat transfer, HFSs have the ability to measure transient heat transfer phenomena. When thin sensors are made of materials with high thermal diffusivity, the sensors can be used to measure fast thermal transients in the submicrosecond regime that many widely available temperature sensors are not suited for because of the mass-dependent thermal inertia. The 98% response time of the sensor in seconds can be calculated based on the conductive heat propagation through the sensor in response to the applied thermal gradient

$$t = \frac{1.5h^2}{\alpha} \tag{3}$$

where h is the sensor thickness in meters and α is the thermal diffusivity in m^2/s [13].

An additional analogy can be drawn between the measurement of electric current based on voltage measurement across a shunt resistance and the measurement of heat current using an HFS [4]. Similar to the measurement of voltage across a shunt resistor, the flow rate of thermal energy can be inferred by measuring the magnitude of the temperature gradient across a heat resistance impeding the flow of heat. However, in the case of thermopile-based heat flux measurement, in addition to increasing the thermal resistance of the sensor, that is, employing materials with a lower thermal conductivity, the sensitivity of the sensor can also be increased by improving the efficiency of the thermoelectric conversion taking place inside the sensor that is responsible for the output signal. The latter method is preferred in many practical heat flux measurement applications because of the desired minimum perturbance in the temperature field of interest [1], and it is the primary approach used in this study.

B. Available Sensor Technology for Contact Measurement

Thermopile HFSs are commonly implemented in the form factor of a plate, Fig. 1, although the materials, geometries, and fabrication methods vary. In addition to the classic plate-type HFSs, heat transfer measurement can be achieved with several other transducer technologies based on the conversion of heat into electricity, including thermopile infrared (IR) sensors, Gardon gauges, Peltier elements, and thermoelectric generators (TEG) [3], [14], [15]. While many thermopile-based transducers, such as TEGs and IR sensors, are widespread in the industry and have low manufacturing costs [14], [15], few of the technologies are well-suited for surface heat flux measurements because of their mechanical or thermoelectric properties. On the other hand, many of the technologies that are better suited for surface heat flux measurement suffer from poor availability and manufacturing difficulties [4].

Traditionally, thermopile designs have been variations of the p- and n-type thermoleg ingot arrangement, where either p- or n-type semiconducting materials, or both, may also be replaced with different metals [15]–[17]. Most thermoelectric generators and Peltier elements are built using the conventional ingot arrangement on a macroscopic scale [15]. Even though such designs have proven to be cost-effective to

manufacture and, because of their size, exhibit a high thermal resistance [15], such designs are typically not optimized for sensor applications. In practical measurement settings, such devices are typically mechanically and thermally ill-suited for heat flux measurement as a result of their large size and mass [4].

The ingot-type thermopile designs have also been taken to the microscale, Fig. 2(a), with devices known as micro thermoelectric generators (μTEG) [15], [17]. Despite the reduced size and increased volumetric performance of μTEGs as compared with conventional TEGs, μTEGs have been optimized for thermoelectric power generation and thus feature a high thermal resistance [15] and relatively slow temporal responses [18]. Despite the thermal and mechanical challenges, μTEGs have been employed for heat flux measurement because of their high sensitivities.

The use of microfabrication methods, such as MEMS, has been found to offer a number of benefits for achieving a high density of thermoelectric junctions in planar-type IR sensors [14], [17], [19]. However, owing to the lateral arrangement of the thermoelectric legs, Fig. 2(b), the IR sensors have an uneven lateral heat distribution by design, which complicates their use in conductive heat flux measurements in the vertical direction [17]. In addition, the suspended thin film devices are fragile [20], further making them impractical for conductive heat flux measurement.

Manufacturing a mechanically robust contact-type HFS with a fast temporal response and a high sensitivity is difficult [4]. An example of a mechanically durable sensor structure is the gradient HFS (GHFS), Fig. 2(c), which incorporates an anisotropic active sensing layer based on a tilted multilayer structure [2]. Such a structure can be mechanically robust in a very wide range of environmental conditions, while achieving favorable operation characteristics and a significantly higher fill rate of the active layer volume than traditional thermopile structures [2], [4]. However, sensors incorporating such structures are currently limited to low manufacturing volumes, as there are no commonly used mass production techniques available for manufacturing them [4].

Vertically arranged microfabricated thermopile sensor structures have been proposed for providing the improved thermal performance required for surface measurements [20], [21]. Such designs typically have higher mechanical durability and a more uniform lateral heat distribution than conventional membrane-type sensors, while the vertical arrangement introduces a potential for high integration densities [17]. However, attaining favorable operational characteristics for vertical HFS designs using cost-effective manufacturing methods, while maintaining high sensitivity, has not yet been accomplished, suggesting that new designs are needed.

III. Sensor Prototype Design

Typically, the design process revolves around simultaneous electrical, thermal, and mechanical optimization, in addition to overarching manufacturability considerations. In the proposed sensor design, the common issues of the high thermal obtrusiveness and slow response time were aimed to be solved by limiting the physical size of the sensor, particularly its thickness, and by employing higher thermal conductivity materials. At the same time, the density and thermopower of the thermoelectric legs were set out to be maximized. Additionally, because the sensors were to be placed in direct mechanical contact with surfaces to be measured, the sensors were designed to be mechanically robust enough for handling and to withstand environmental effects. The proposed sensor was designed to be fabricated by using MEMS methods.

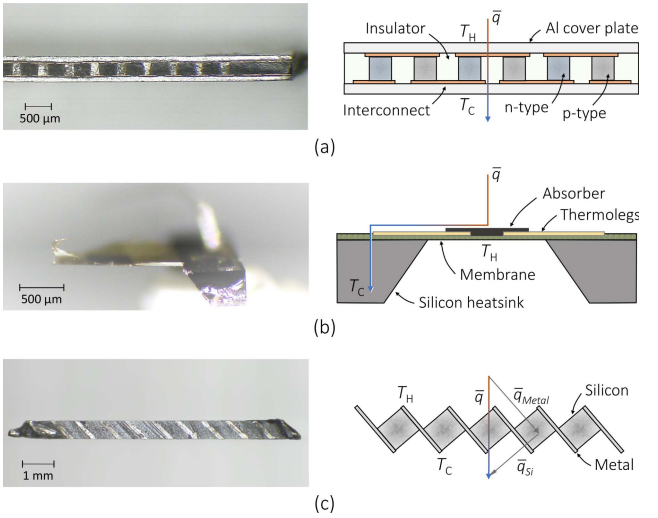

Fig. 2. Cross-sectional micrographs of common thermopile sensors with their operational schematics, showing the hot and cold junctions T_H and T_C, the path of heat flux $\overline{q}$, and component parts of sensors. (a) Commercial μTEG based on the traditional p- and n-type ingot structure. (b) Conventional membrane-type MEMS IR thermopile. (c) Si-Al tilted multilayer GHFS.

A. Design Optimization

The design process of an HFS is slightly different from that of TEG systems. For one, the thermoelectric performance of the sensor is focused on generating a high open-circuit electric potential, rather than power generation [1], [14]. Thus, the thermoelectric design of the sensor focuses largely on high Seebeck coefficient materials, with more relaxed requirements for the electrical resistivity of the thermopiles. Although a reasonably low source resistance is beneficial in reducing noise and interference of the measurement, relatively large resistances in excess of tens of kilo ohms have still been viewed as acceptable for sensing purposes [14].

In addition to maximizing the Seebeck coefficients of the individual thermolegs, an increased sensitivity per unit sensor area is achievable by increasing the integration density of thermolegs [14]. To this end, the entire sensing layer volume should be employed as effectively as possible as a thermoelectric transducer [4]. Moreover, since the entire thermoleg height in the direction of the temperature gradient is responsible for the generation of the electromotive force, the thermolegs should be oriented codirectionally with the heat flow [1].

Another significant design point is the thermal resistance of the sensor, in terms of both transient and steady-state performance [1], [17]. While in both the IR detector and TEG designs the thermal resistance across the device is aimed to be kept very high to ensure a large temperature difference

across the thermopile [17], the same is not necessarily ideal for the case of HFSs. Because the HFS works by passing the heat current through the sensor itself, the sensor inherently becomes a part of the measured thermal system [1]. Thus, introducing a high thermal resistance onto a surface can be detrimental to the measurement accuracy or repeatability by impacting the temperature field at the site of the sensor [1].

Because most thermopile designs aim for high temperature differences across the thermoelectric active layer, typical thermopile sensors have traditionally exhibited slow response times on the order of milliseconds to seconds [4], [18]. As seen in (3), the thickness of the sensor has a quadratic dependence on response time, and should thus be kept low, in addition to using high thermal diffusivity materials. However, as demonstrated in [17], the use of a thin vertical active layer in a thermoelectric transducer may result in an increased proportion of temperature drop across the sensor to occur at thermal contact interfaces. Thus, tradeoffs between the thermal resistance and the sensitivity of the sensor were unavoidable in the design process.

To ensure high performance of the prototype sensors, the design in this article was based on a high topography micromachined structure, with monocrystalline silicon as the base sensing layer material. Having a high thermal conductivity, the use of bulk crystalline silicon facilitated the formation of tall structures by anisotropic etching, with good controllability of the features made. In addition to its high thermal conductivity, the use of silicon also facilitated the formation of tall structures via crystalline-based anisotropic etching. In practice, the thermal resistance layer was implemented by anisotropic etching of an array of mesa-shaped structures into silicon. Owing to the orientation-dependent etching of silicon, the formed mesa structures with slanted sidewalls also favored subsequent deposition of thermoelectric layers [20].

An obvious shortcoming of the increased height of silicon was the reduced density of thermolegs, resulting from the limited aspect ratio of the etching processes available. However, the resulting increased structural dimensions were considered beneficial for early prototyping purposes. In addition to practical advantages, such as easier access to the silicon structures for bonding and thermal tests, the large contact areas helped in realizing ohmic contacts with low electrical resistances.

A vertically configured MEMS thermopile with a similar design basis was developed by the group of Huynh *et al.* [20]. In the design, they used 7-μm deep trenches etched to monocrystalline silicon as the thermal resistance of the sensor, followed by deposition of metallic thermoelectric legs. Such a design in its current form was, however, estimated to require too large die areas for sufficient sensitivity because of the low Seebeck coefficients of the metal thermolegs used in the design, and therefore, another approach was chosen.

In the present design, the relative volumes of the nonthermoelectric materials were set out to be minimized. Consequently, the etched mesa structures were employed as a part of the thermoelectric circuit of the sensor, simultaneously acting as the mechanical support and the thermal resistance layer. To facilitate the electrical series connection of the mesa structures, the device was designed to be made on

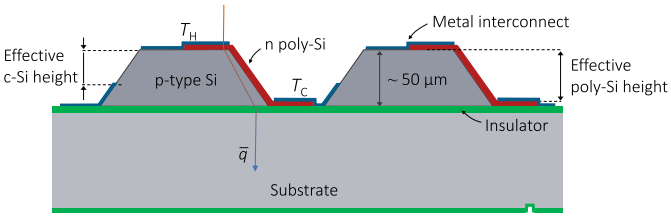

Fig. 3. Cross-sectional schematic showing the thermoelectric operation principle of the proposed thermopile structure in response to the heat flux $\overline{q}$, with the hot and cold junctions T_H and T_C shown.

silicon-on-insulator (SOI) wafers, where the entire device layer was employed for the thermopile construction. The design was made on p-type device SOI wafers with a relatively low dopant concentration because of the inherent large thickness of the thermolegs leading to a low sheet resistance and the high Seebeck coefficient of bulk p-type silicon [14].

Polysilicon was chosen as the second thermoelectric material because of its significantly higher Seebeck coefficient than that of metals [13], [14]. Furthermore, employing n-type polysilicon as the second thermoleg material was beneficial for improving both the sensitivity and geometric simplicity of the design: while polysilicon had a higher Seebeck coefficient and a lower thermal conductivity than those of metals, the polysilicon did not require any electrical insulation from the p-type mesas. Finally, a layer of aluminum was used to connect the top and bottom junctions at the top and bottom contact junctions of the mesa structures to complete the thermopile. The finalized sensor structure is illustrated in Fig. 3.

Further restrictions for the sensor geometry design were introduced by the applied MEMS fabrication processes. The device construction was based on a high topography surface, with mesa structures of 50 μm height formed on the SOI substrate. Due to the nature of silicon (111) crystalline sidewall angles from the tetra-methyl-ammonium hydroxide (TMAH) wet etching, the mesa dimensions and spacing had to be increased to ensure suitability for further processing.

As a consequence of the top-down process flow, the contact to the bottom side of the mesa structures had to be made on the lower part of the mesa sidewalls so that a small portion of the effective thermoleg height had to be sacrificed, Fig. 3. Across the structure, the coverages of polysilicon and aluminum were compromised between creating large enough contact areas and maximizing the effective vertical height of the device without electrical short-circuiting of the legs, see Figs. 3 and 4.

Finite element modeling was performed on the proposed sensor structure to verify its operation prior to prototype manufacturing. The thermopile structure was modeled in a 2-D setting with similar dimensions to those of the prototype sensors. The p-type mesa structures were modeled with a 50 μm height, a top plane width of 80 μm, a sidewall angle of 54.7°, and an out-of-plane thickness of 300 μm. The modeling was performed on Comsol Multiphysics with parameters shown in Table I. The results, illustrated in Fig. 5, showed that the structure works as a thermopile and generates an electric potential of 0.4 μV per p-n pair of thermolegs in response to a vertical temperature difference of 1 millikelvin across the structure.

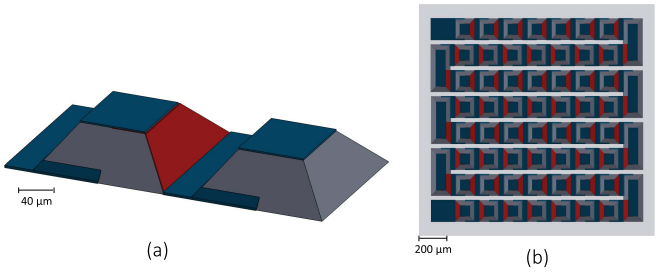

Fig. 4. Schematic 3-D illustration of the proposed sensor structure. (a) Electrical contacts around mesa structures. (b) Top view of a sensor showing a series-connected meander of thermolegs formed and bondpads. Relative polysilicon and metal layer coverages are shown. Compromises were made between maximizing both the silicon-to-metal contact interface areas and the effective vertical thermoleg height.

TABLE I
PARAMETERS USED FOR THE FINITE ELEMENT MODEL OF THE SENSOR

Section	Parameter	Value
p-type thermolegs	Thermal conductivity	130 W/(m · K)
	Electrical conductivity	75 S/m
	Seebeck coefficient	500 µV/K
Poly-Si layer	Thickness	5 µm
	Thermal conductivity	30 W/(m · K)
	Electrical conductivity	3000 S/m
	Seebeck coefficient	-300 µV/K
Al interconnets	Thickness	3 µm
	Thermal conductivity	237 W/(m · K)
	Electrical conductivity	35.5 MS/m
	Seebeck coefficient	-1.5 µV/K

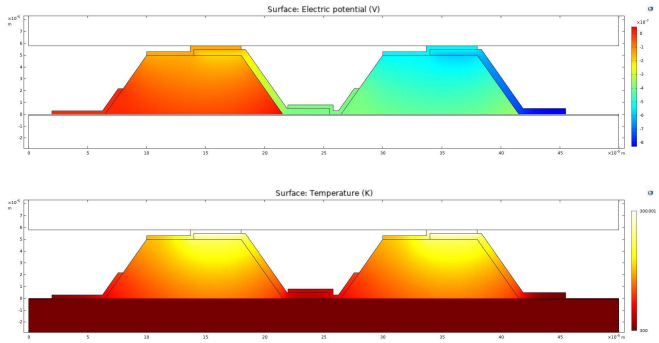

Fig. 5. Proposed sensor structure modeled two-dimensionally by the finite element method, showing a total electric potential of 0.8 μV across four thermolegs in response to a temperature difference of 1 millikelvin, with the temperature field shown. In the temperature field plot, hot and cold junctions can be observed at the top and bottom of the mesa, respectively. The dimensions of the polysilicon and metal layers are not to scale; the resulting voltage is less than 0.5% higher than obtained with actual thinner layer thickness values.

B. Prototype Manufacturing Process

A prototype batch of HFSs was manufactured onto 6-in SOI silicon wafers with a 50-μm-thick device layer. Anisotropic wet etching was used to form an array of mesa structures into the device layer. By depositing and patterning a polysilicon and aluminum interlayer on top of the mesa structure, a vertically configured 3-D thermopile device was constructed. Additionally, the sensor surface was passivated with SiO_2, and the aluminum contact pads were revealed by etching a window through the passivation oxide. The process flow, Fig 6, comprised of the following steps.

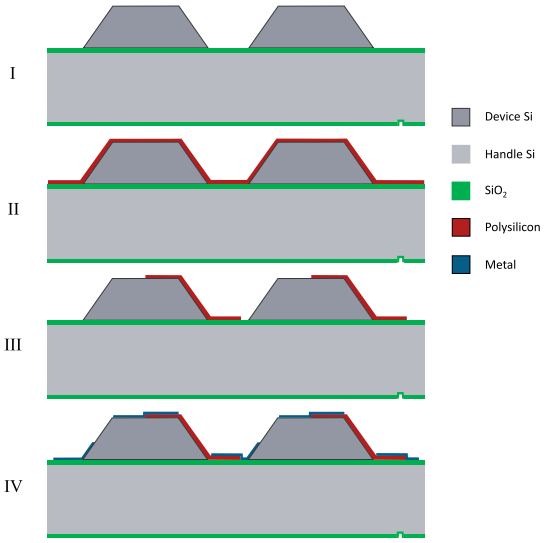

Fig. 6. Main processing steps of the fabricated sensor prototype. I: Anisotropic etching was used to form an array of mesa structures doubling as thermal resistance and p-type thermolegs. II: Polysilicon layer deposition. III: Patterning of the polysilicon layer to form n-type thermolegs along the mesa sidewall. IV: Patterning of aluminum interconnects to form a thermopile.

1) Starting with SOI wafers.
2) Oxidation to form SiO_2 mask for TMAH etching.
3) Oxide mask patterning.
4) Mesa etching in TMAH and mask removal (I).
5) Polysilicon layer deposition (II).
6) Polysilicon layer patterning (III).
7) Metal layer deposition.
8) Metal layer patterning (IV).
9) Passivation oxide deposition.
10) Contact pad patterning.

IV. RESULTS AND DISCUSSION

The manufactured sensor prototype operates similar to a conventional thermopile. The measured temperature gradient of interest is imposed across the SOI active layer, which incorporates electrically series-connected thermoelectric legs of p- and n-type silicon for transducing the signal. In such a configuration, in addition to forming the heat resistance layer, the device layer silicon bulk material contributes to the voltage response of the sensor. The vertical monocrystalline silicon structure reduces the heat resistance in comparison with conventional HFS designs, leading to reduced thermal disturbance of the measured systems and a significantly faster response time as compared with sensors of similar sensitivities.

A. Fabrication Results

The manufacturability of the proposed design was conceptually proven in a successful processing run. Even though further work on optimizing the structure and the processing is still required, it was shown that a high-topography vertical HFS design can be implemented on SOI wafers using widely available basic MEMS processes. The finished thermoelectric structure of the prototype sensors is shown in Figs. 7 and 8.

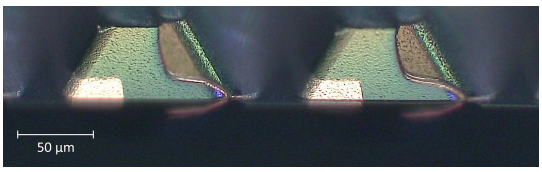

Fig. 7. Side view micrograph of the fabricated HFS prototype showing silicon mesa structures with deposited polysilicon and metal layers.

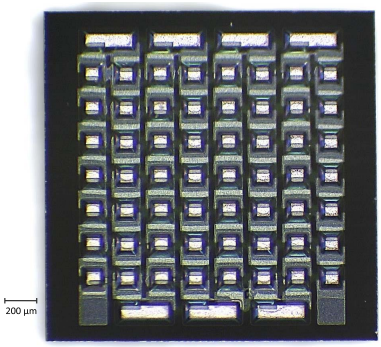

Fig. 8. Top view of the fabricated HFS prototype, showing a series-connected meander of silicon thermolegs. Because of the lithography challenges introduced by the high topography surface of the sensor, short-circuits of polysilicon were observed on several prototypes.

Challenges arose in the effective lithography resolution during the prototype fabrication process because of the high topography surface of the sensors, at 50 μm above the substrate surface. The high mesa structure height and the slanting sidewalls made photoresist coating challenging. In addition, patterning of the resist required precise control of the compounding effects of the exposure and development processes to ensure that excess openings were not formed at the top and that sufficient openings were formed at the bottom. Because of the lithography challenges, the critical dimensions, in other words, the feature size of the polysilicon and metal layers, were limited to a large extent to ensure the functionality of the prototypes. Despite the increased structural dimensions, a number of prototypes still exhibited occasional short-circuits in the polysilicon layer, Fig. 8, suggesting a need for further optimization of the sensor structure and the processing steps.

B. Sensor Characterization

The operation of the manufactured sensor prototype was validated in two different characterization tests. First, the volt-watt sensitivities of the sensors were recorded on the wafer level during electrothermal characterization in a relative test setting. Next, the temporal responses of four wire-bonded sensors were assessed in a second test setup. In addition, the series resistances of the prototypes were measured to be in the range of 400–700 Ω.

A stacked structure incorporating the devices under test (DUT) and a calibrated reference sensor (greenTEG gSKIN XM) [18] was constructed into a wafer probing station to perform relative sensitivity tests, Fig. 9.

Wafer-level electrothermal characterization was performed by conducting heat periodically in both directions through the test structure of Fig. 9 during a 12 min test sequence. The thermal excitation signal was induced as a combination of

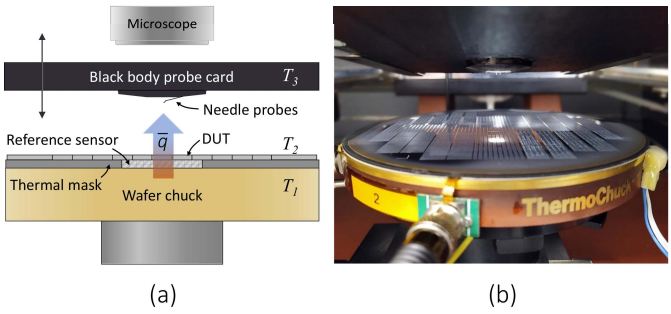

Fig. 9. Relative sensitivity characterization setup with four reference HFSs situated under the DUT wafer. (a) Schematic illustration and (b) photograph of the test setup. Blackbody radiator with needle probes is lowered onto the wafer to test the DUT sensitivities. Additionally, temperatures of the chuck surface, the wafer surface, and the blackbody, denoted by T_1, T_2, and T_3, respectively, were recorded.

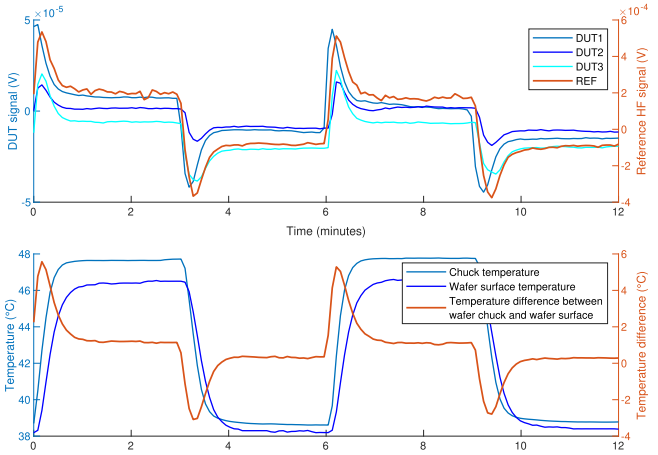

Fig. 10. Output signals of the tested sensors (DUTs 1–3) recorded during a sequence of bidirectional thermal excitation, compared with a reference heat flux signal from the calibrated sensor REF placed under the DUTs. Temperatures of the wafer chuck and the wafer top surface were recorded for control purposes. Operation of the HFSs is further validated by the calculated temperature difference.

conductive and radiative heat between a thermal wafer chuck and a blackbody probe card assembly. The electrical responses of the DUT sensors located adjacent to one another on the SOI wafer were recorded and their output compared with a reference sensor located under the DUTs to ensure as equal thermal conditions as possible. During the excitation sequence, the transient and quasi-steady-state heat flux signals of both the DUTs and the reference sensor were recorded. In addition, the temperatures of the wafer chuck surface, the wafer surface, and the blackbody were recorded for control purposes. The construction and operation of the test setup are discussed in detail in [22]. Example heat flux and temperature waveforms obtained from 3 of the tested sensors are shown in Fig. 10.

All of the tested sensors produced a waveform similar to that of the reference sensor, with slightly differing transient responses likely owing to differing thermal properties and contacts of the sensors. The DUT output signal waveforms followed the output signal of the reference sensor relatively closely, considering the partly unknown thermal contacts to the DUT sensors on the top side, which are presumably the largest contributor to the observed discrepancies between the

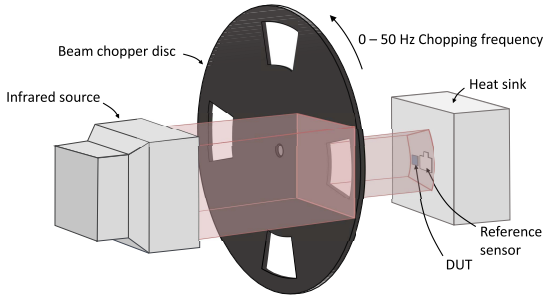

Fig. 11. Schematic illustration of the test setup used for comparing temporal responses of the DUTs and the commercial reference sensor. An optical beam chopper was used to modulate infrared sensor excitation in the range of 0–50 Hz.

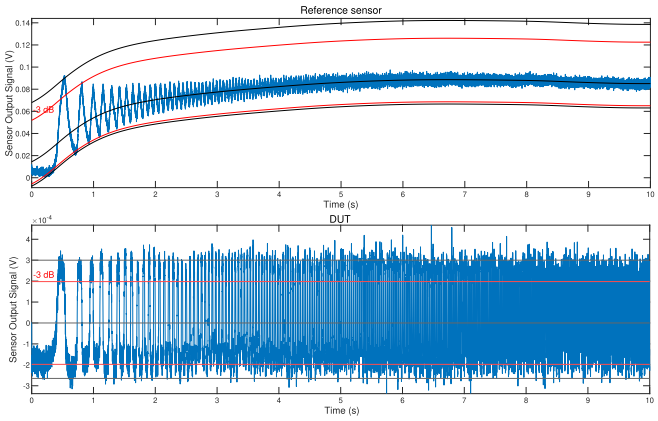

Fig. 12. Comparison of the relative amplitudes of the reference sensor and the DUT in response to chopped infrared excitation in the frequency range of 0–50 Hz. The maximum and −3-dB amplitudes are shown in black and red, respectively. The reference sensor showed 3-dB attenuation before 3.5 Hz, while the amplitude of the DUT output did not show a noticeable attenuation in the tested frequency range.

measured waveforms. The difference in the measured signal baseline is also probably resultant from differing conditions of the thermal contacts and masses of the test setup components.

As seen in Fig. 10, the tested sensors exhibit appropriate responses of both positive and negative output voltages in response to bidirectional heat flux excitation. The average peak-to-peak quasi-steady-state values of the reference sensor were calculated to be 270 μV, while for DUTs, the corresponding values were in the range of 18–28 μV. Considering the sensitivity value of 1.5 V $\cdot$ mm^2/W of the reference sensor [18], the sensitivities of the DUTs were estimated to be in the range of 0.1–0.19 V $\cdot$ mm^2/W. For their commercial counterparts of 2 mm $\times$ 2 mm, a sensitivity of 0.3 V $\cdot$ mm^2/W was reported [18]. It should also be noted that a calculation mistake was made in our early results proceedings article regarding the sensitivity [12]. Instead of 1.5 V $\cdot$ mm^2/W, a typical sensitivity value of 0.15 V $\cdot$ mm^2/W was observed.

Because the sensitivity of a HFS depends on the number of thermolegs fitted inside the sensor, the sensitivities of the sensors should be compared in relation to their surface areas. The surface area-dependent sensitivity, that is, volt-watt sensitivity, was measured to be typically at 55 mV/W, whereas the corresponding value for the reference sensor was 77 mV/W. Other HFS designs reported in the literature have comparable or greater sensitivities of up to 65 mV/W for the bismuth-based GHFS [4], 63 mV/W for the design of [20], and 180 mV/W for the lateral CMOS design of [19].

The temporal responses of the sensor prototype and a commercial HFS (greenTEG gSKIN XP) [18] were compared in a simple radiative test setting. The tested sensors were mounted to a large heat sink, and a ceramic infrared heater at a temperature of 400 °C was placed at a distance of 20 mm from the sensors. A rotating disk optical chopper was placed between the sensors and the infrared source to modulate the infrared excitation, Fig. 11. The output signals of four DUTs and the reference sensor in response to chopped infrared excitation in the frequency range of 0–50 Hz were recorded and their relative amplitudes compared. The recorded waveforms of the reference sensor and one of the tested DUTs during a 10 s test are shown in Fig. 12.

The response times of the sensors were compared based on the relative amplitudes of the output signals of the sensors during the chopped infrared irradiation test. The breakpoint of the thermal low-pass filter formed by the sensor structure was estimated by calculating the excitation frequency at the attenuation level of −3 dB. The commercial sensor showed a 3-dB attenuation of its output signal amplitude before the chopping frequency of 3.5 Hz, while none of the DUTs showed signs of frequency-dependent attenuation in the tested range.

These results suggest that the manufactured prototype sensors have a significantly faster response time than that of the reference sensors. Assuming a thermal diffusivity value of 88 mm^2/s for the silicon active layer [23], according to (3), the prototype sensors have a theoretical 98% response time of approximately 43 μs. Verifying the maximum response time of the sensors, however, requires a significantly improved test setup and is thus a matter of further study.

C. Discussion

Based on the conducted early measurements, the developed sensors are expected to have an equal or slightly lower sensitivity, but significantly improved thermal characteristics as compared with similarly sized commercial plate-type HFSs. Because the developed prototype sensors still require wire bonding and application of top-side cover plates, further tests should be performed after the mechanical assembly process is completed. This is due to the fact that the thermal properties of the topside encapsulation process will unavoidably have an effect on both the sensitivity and the frequency response of the sensor.

Further optimization and prototyping are required to improve performance and manufacturability. Densifying the sensor structure may be considered to improve the design sensitivity in future design iterations. Because of the slightly exaggerated dimensions of the present design, the arrangement of the structure could be further densified, and an increased proportion of the die area could be employed.

The benefits of decreasing the relative dimensions of the mesa structures and increasing the employed die area are twofold. First, an increased die area and structure packing density result in an increased number of thermolegs and thus, increased sensitivity. Secondly, decreasing the top-plane

contact area would probably benefit the design by decreasing the total mesa top-plane area, thereby increasing the relative vertical temperature difference across the mesa structures. In addition to densifying the sensor structure itself, the design could probably benefit from a reduction of the device layer height so that more precise lithography and an increased thermoleg count would be possible.

Depending on the eventual application of the sensors, different variations of the design could be realized to achieve improved sensitivity or higher tolerance of environmental effects. In addition to improving the sensor's thermoleg packing density, the sensitivity of the sensor could be further improved by material choices. For example, the deposited layers could be made of materials with higher Seebeck coefficient or lower thermal conductivity, such as silicon in its polycrystalline or porous forms. However, the current manufacturing process limits the supporting mesa structure to monocrystalline silicon.

The promising prototype fabrication and test results suggest that the proposed HFS design is potentially scalable for mass production, while exhibiting suitable thermoelectric performance and adequate mechanical properties required by typical surface measurement applications. Manufacturing a cost-effective HFS using MEMS is an important step toward realizing integrated HFS chips suitable for conductive heat flux measurement. Such a chip could find multiple uses in smart measurement systems, for example, in wearables, energy storage devices, and power electronics monitoring.

The present sensor structure was designed specifically for contact-type heat flux measurement, which in combination with the potentially low fabrication costs enables improved or new HFS applications. Previously, the widespread use of HFSs has been limited by the mechanical or thermoelectric properties of the existing technology, along with difficult manufacturability, leading to the use of more readily available temperature sensors, and, in turn, reduced awareness of the HFS capabilities. However, improving the performance, availability, and fabrication costs of HFSs has the potential to facilitate new or improved measurement methodologies in a variety of thermal measurement applications.

As HFSs produce an output signal directly proportional to the flow rate of heat, the sensors can be used in advantageous ways in several applications where several modes of heat transfer, that is, conduction, convection, or radiation, exist or the use of multiple temperature sensors is impractical. This is also demonstrated in Fig. 10, where the HFSs directly provide the same information that was obtained by calculation based on outer and inner temperatures of the structure. Practical examples of applications where it may be more practical to use HFSs include unobtrusive estimation of inner temperatures of objects, for example, the measurement of human body core temperature from the skin surface [8], measurement of microsecond-range thermal transients [2], or differential temperatures [1].

The significantly decreased thermal resistance over conventional designs and similar volt-watt sensitivity of the present sensor design suggests that the sensors could have potential uses in differential temperature measurement applications. Based on (2) and Fourier's law, a temperature difference of 1 μK would result in a heat flux of 2.6 W/m^2 across the sensing layer of the proposed sensor, with a differential output voltage of approximately 0.4 μV. However, the usability of the sensor for such an application still remains to be explored.

Successfully implemented vertical sensor designs also have the potential to ease the construction process of thermoelectric devices in both sensing and thermoelectric generator solutions. For one, the use of thermoelectric elements could find uses in autonomous wireless sensor nodes [16], where the thermoelectric transducers could in addition to power generation also double as a sensor element. Furthermore, the introduction of an easily manufacturable vertical thermopile structure can significantly reduce the volumetric proportion of the filler materials in TEG designs, such as the vertical-to-lateral heat guide structures and thermally and electrically insulating materials presented in [16]. The proposed series-connected mesa geometry can also be applied to different processes, ranging from TEG constructions to infrared sensors, by enabling simple vertical arrangement of thermolegs.

V. Conclusion

A MEMS-compatible surface HFS was successfully designed, fabricated, and tested. The characterization results show that the developed sensors have a surface-area-dependent sensitivity and response time comparable with commercial HFSs.

The proposed fabrication method is compatible with basic MEMS processes, and thus suggests a possibility of cost-effective mass production of the sensors. This is an important step toward making heat flux measurements more widely available for high-volume applications, where a calibrated integrated HFS chip could ease the measurement of thermal energy transfer. Furthermore, owing to the implemented vertical structure, the proposed sensor is mechanically durable and thermally suitable for surface-mount use. These advantages facilitate the use of HFSs in applications around thermal monitoring and energy efficiency, for example, in wearable electronics and IoT.

Acknowledgment

The authors would like to thank VTT Technical Research Centre of Finland Ltd. for contribution to the project with the fabrication of the sensor prototype batch at Micronova, and greenTEG AG for providing the calibrated reference sensors.

References

[1] P. Childs, J. Greenwood, and C. Long, "Heat flux measurement techniques," *Proc. Inst. Mech. Eng., C, J. Mech. Eng. Sci.*, vol. 213, no. 7, pp. 655–677, 1999.

[2] A. V. Mityakov, S. Z. Sapozhnikov, V. Y. Mityakov, A. A. Snarskii, M. I. Zhenirovsky, and J. J. Pyrhönen, "Gradient heat flux sensors for high temperature environments," *Sens. Actuators A, Phys.*, vol. 176, pp. 1–9, Apr. 2012.

[3] A. Murthy, B. K. Tsai, and R. D. Saunders, "High-heat-flux sensor calibration using black-body radiation," *Metrologia*, vol. 35, no. 4, p. 501, 1998.

[4] S. Z. Sapozhnikov, V. Y. Mityakov, and A. V. Mityakov, *Heatmetry: The Science and Practice of Heat Flux Measurement*. Cham, Switzerland: Springer, 2020.

[5] P. Godts, D. Dupont, and D. Leclercq, "Direct measurement of the latent heat of evaporation by flowmetric method," *IEEE Trans. Instrum. Meas.*, vol. 54, no. 6, pp. 2364–2369, Dec. 2005.
[6] Y. Zhang and T. M. Jahns, "Power electronics loss measurement using new heat flux sensor based on thermoelectric device with active control," *IEEE Trans. Ind. Appl.*, vol. 50, no. 6, pp. 4098–4106, Nov. 2014.
[7] S. Levikari *et al.*, "Improving energy expenditure estimation in wearables using a heat flux sensor: First observations," presented at the IEEE Int. Instrum. Meas. Technol. Conf. (I2MTC), Dubrovnik, Croatia, May 2020.
[8] L. Atallah *et al.*, "Perioperative measurement of core body temperature using an unobtrusive passive heat flow sensor," *J. Clin. Monitor. Comput.*, vol. 34, pp. 1351–1359, Jan. 2020.
[9] R. Rizk, H. Louahlia, H. Gualous, P. Schaetzel, and G. Alcicek, "Experimental analysis on Li-ion battery local heat distribution," *J. Thermal Anal. Calorimetry*, vol. 138, no. 2, pp. 1557–1571, Oct. 2019.
[10] M. Frei, J. Hofer, A. Schlüter, and Z. Nagy, "An easily-deployable wireless sensor network for building energy performance assessment," *Energy Procedia*, vol. 122, pp. 523–528, Sep. 2017.
[11] M. Collins, K. Chana, and T. Povey, "New technique for the fabrication of miniature thin film heat flux gauges," *Meas. Sci. Technol.*, vol. 26, no. 2, Feb. 2015, Art. no. 025303.
[12] A. Immonen, S. Levikari, F. Gao, M. Kuisma, and P. Silventoinen, "MEMS heat flux sensor," presented at the IEEE Int. Instrum. Meas. Technol. Conf. (I2MTC), Dubrovnik, Croatia, May 2020.
[13] P. R. Childs, *Practical Temperature Measurement*. Amsterdam, The Netherlands: Elsevier, 2001.
[14] D. Xu, Y. Wang, B. Xiong, and T. Li, "MEMS-based thermoelectric infrared sensors: A review," *Frontiers Mech. Eng.*, vol. 12, no. 4, pp. 557–566, Dec. 2017.
[15] J. Yan, X. Liao, D. Yan, and Y. Chen, "Review of micro thermoelectric generator," *J. Microelectromech. Syst.*, vol. 27, no. 1, pp. 1–18, Feb. 2018.
[16] T. N. Huu, T. N. Van, and O. Takahito, "Flexible thermoelectric power generator with Y-type structure using electrochemical deposition process," *Appl. Energy*, vol. 210, pp. 467–476, Jan. 2018.
[17] W. Glatz, S. Muntwyler, and C. Hierold, "Optimization and fabrication of thick flexible polymer based micro thermoelectric generator," *Sens. Actuators A, Phys.*, vol. 132, no. 1, pp. 337–345, Nov. 2006.
[18] GreenTEG. (2020). *Heat Flux Sensor gSKIN Series Datasheet*. Accessed: Mar. 9, 2020. [Online]. Available: https://shop.greenteg.com/heat-flux-measurement-heat-flux-sensor-gskin-xm/
[19] K. Ziouche, P. Lejeune, Z. Bougrioua, and D. Leclercq, "Dispersion of heat flux sensors manufactured in silicon technology," *Sensors*, vol. 16, no. 6, p. 853, Jun. 2016.
[20] T. Huynh, Y. Zhang, and C. Yehuda, "Fabrication and characterization of a multichannel 3D thermopile for chip calorimeter applications," *Sensors*, vol. 15, no. 2, pp. 3351–3361, Feb. 2015.
[21] M. Lindeberg, H. Yousef, H. Rödjegård, H. Martin, and K. Hjort, "A PCB-like process for vertically configured thermopiles," *J. Micromech. Microeng.*, vol. 18, no. 6, 2008, Art. no. 065021.
[22] A. Immonen, "A heat flux sensor test setup," M.S. thesis, School Energy Syst., Lappeenranta Univ. Technol., Lappeenranta, Finland, 2019. [Online]. Available: http://urn.fi/URN:NBN:fi-fe2019090927472
[23] J. Wilson, "Thermal diffusivity," *Electron. Cooling*, vol. 13, no. 3, p. 7, 2007.

Antti Immonen (Member, IEEE) was born in Finland in 1993. He received the B.Sc. and M.Sc. degrees from LUT University, Lappeenranta, Finland, in 2018 and 2019, respectively, where he is currently pursuing the Ph.D. degree with the LUT School of Energy Systems, Laboratory of Applied Electronics.

His main research topics include thermoelectric devices, sensors, and biophysical instrumentation.

Saku Levikari (Member, IEEE) was born in Finland in 1991. He received the B.Sc. and M.Sc. degrees from the Lappeenranta University of Technology (LUT), Lappeenranta, Finland, in May and June 2018, respectively, where he is currently pursuing the Ph.D. degree with the LUT School of Energy Systems, Laboratory of Applied Electronics.

His research interests are in the field of data analytics and machine learning, with topics ranging from biosignal measurements to power electronics reliability.

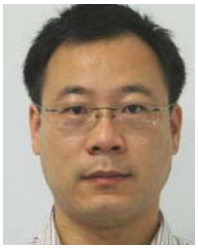

Feng Gao was born in China in 1977. He received the B.E. degree in photoelectronics and information engineering from Shandong University, Shandong, China, in 2000, and the M.Sc. degree in micro and nanotechnology from the Helsinki University of Technology, Helsinki, Finland, in 2006.

He has worked with the VTT Technical Research Centre of Finland Ltd., Espoo, Finland, since 2005. His research interests include deep reactive ion etching (DRIE) and general process integration of silicon based microelectromechanical system (MEMS) devices.

Pertti Silventoinen (Member, IEEE) was born in Simpele, Finland, in 1965. He received the M.Sc. degree in electrical engineering, the Licentiate of Technology degree in applied electronics and control systems, and the Ph.D. degree in science, focusing on EMC in electronics from the Lappeenranta University of Technology (LUT University), Lappeenranta, Finland, in 1993, 1997, and 2001, respectively.

Since 2008 he has been a Full Professor in applied electronics at LUT University. His research interest includes analog signal processing and measurement systems, power line communication applications, EMC measurement technology and power electronic systems in various forms.

Mikko Kuisma (Member, IEEE) was born in Finland, in 1971. He received the M.Sc. degree in electrical engineering and control systems and the D.Sc. degree in electronics from the Lappeenranta University of Technology (LUT), Lappeenranta, Finland, in 1997 and 2004, respectively.

He became an Associate Professor of applied electronics with the Department of Electrical Engineering, LUT University in 2002. Since 1995, he has been working in the field of electronics, sensors, acoustics, IoT, EMC, and engineering education. His current research interests include measurement electronics and sensors in various applications.